arXiv:1606.08816v2 [cond-mat.stat-mech] 17 Aug 2016

Two-site Bose-Hubbard model with nonlinear tunneling: classical and quantum analysis

D. Rubeni, J. Links and P. S. Isaac
School of Mathematics and Physics, The University of Queensland, Brisbane, QLD 4072, Australia

A. Foerster
Instituto de Física da UFRGS, Av. Bento Gonçalves 9500, Agronomia, Porto Alegre, RS, Brazil

The extended Bose-Hubbard model for a double-well potential with atom-pair tunneling is studied. Starting with a classical analysis we determine the existence of three different quantum phases: self-trapping, phase-locking and Josephson states. From this analysis we built the parameter space of quantum phase transitions between degenerate and non-degenerate ground states driven by the atom-pair tunneling. Considering only the repulsive case, we confirm the phase transition by the measure of the energy gap between the ground state and the first excited state. We study the structure of the solutions of the Bethe ansatz equations for a small number of particles. An inspection of the roots for the ground state suggests a relationship to the physical properties of the system. By studying the energy gap we find that the profile of the roots of the Bethe ansatz equations is related to a quantum phase transition.

I. INTRODUCTION

The Bose–Hubbard model for a double-well potential has been extensively studied since the experimental realization of Bose–Einstein condensates (BECs). This simple model can well describe the Josephson oscillations and nonlinear self-trapping of BECs in a double-well trap [1] with weak atom–atom interactions. Due to its simplicity, this model has been investigated widely by many authors using various methods, such as the Gross-Pitaevskii approximation [2], mean-field theory [3, 4], the quantum phase model [5] and the Bethe ansatz method [6], providing insights into many intriguing phenomena. For example, it is well known that this model may present a *Quantum Phase Transition* (QPT) separating a delocalised from a self-trapped phase [7, 8].

However, strong interaction may fundamentally alter the tunnel configuration and result in a correlated tunnelling, which was explored most recently in the context of ultracold atoms [9, 10]. The tunnelling dynamics of a few atoms loaded in a double-well trap has been studied by varying the interaction strength from a weak to strong limit and it was shown for the two-atom case that the tunnelling character changes from Rabi oscillation to an atom-pair co-tunnelling process with increasing interaction. A direct observation of the correlated tunnelling was reported recently [9] and theoretical analysis has also been presented in terms of two-body quantum mechanics [10]. It was shown that the two-mode Bose-Hubbard model (TMBH) should be modified by a nonlinear interaction-dependent tunnelling term in the case of a large number of atoms [11], which leads to a considerable contribution to the tunnelling effect. In [12], it was pointed out that the Bose–Hubbard Hamiltonian, which is valid in a relatively weak interaction regime, is not able to describe the dynamics of atom-pair tunnelling and should be extended in the strong interacting regime to include the atom–atom interaction of neighbouring lattice sites. In the model under consideration, a novel atom-pair hopping term is included to describe the two-body interaction recently reported experimental observation of correlated tunnelling. There has been a great deal of effort devoted to this subject recently [13–17].

In this paper, we adopt a Hamiltonian including the atom-pair tunnelling term to describe BECs in a double well potential. The extended two-mode Bose-Hubbard model (eTMBH) can be described by the following Hamiltonian

$$H = U_1\hat{n}_1^2 + U_2\hat{n}_2^2 - \frac{1}{2}\Delta\left(\hat{n}_1 - \hat{n}_2\right) - \frac{J}{2}\left(\hat{a}_1^\dagger\hat{a}_2 + \hat{a}_2^\dagger\hat{a}_1\right) - \frac{\Omega}{2}\left(\hat{a}_1^\dagger\hat{a}_1^\dagger\hat{a}_2\hat{a}_2 + \hat{a}_2^\dagger\hat{a}_2^\dagger\hat{a}_1\hat{a}_1\right), \quad (1)$$

where $\left\{\hat{a}_j,\, \hat{a}_j^\dagger | \, j = 1,\, 2\right\}$ are the creation and annihillation operators for well j associated, respectively, with two bosonic Heisenberg algebras, and satisfying the following commutation relations

$$\left[\hat{a}_i,\, \hat{a}_j^\dagger\right] = \delta_{ij},\, [\hat{a}_i,\, \hat{a}_j] = \left[\hat{a}_i^\dagger,\, \hat{a}_j^\dagger\right] = 0.$$

Also $\hat{n}_j = \hat{a}_j^\dagger\hat{a}_j$ is the corresponding boson number operator for each well. Since the Hamiltonian commutes with the total boson number operator $\hat{n} = \hat{n}_1 + \hat{n}_2$, the total number of bosons n is conserved and it is convenient to restrict to a subspace of constant n. The coupling U_j provides the strength of the scattering interaction between bosons in the well j and may be attractive ($U_j < 0$) or repulsive ($U_j > 0$). The parameter Δ is the external potential which corresponds to an asymmetry between the condensates, J is the coupling for the tunneling and Ω is a factor to describes the atom-pair tunneling process. The change $J \to -J$ corresponds to the unitary transformation $\hat{a}_1 \to \hat{a}_1$, $\hat{a}_2 \to -\hat{a}_2$, while $\Delta \to -\Delta$ corresponds

to $\hat{a}_1 \leftrightarrow \hat{a}_2$. Therefore we will restrict our analysis to the case of J, $\Delta \geq 0$.

Undertaking a classical analysis we obtain the fixed points of the system in the large n limit, and find three distinct phases for the ground state. Under the right conditions the system may undergo a QPT. The results for some particular cases allow us to identify a parameter space of quantum phase transitions. We then confirm that this parameter space is associated with quantum phase transitions of the system through studies of the energy gap.

Then we present the exact solution for this model using the Bethe ansatz approach. By this method one can have access to the ground state through the solution of a set of Bethe ansatz equations. A careful observation of the behavior of solutions of these equations for the ground state, as we vary some parameters of the Hamiltonian, suggests a connection between the behavior of roots of the Bethe ansatz equations and the physical behavior of such model. This is exactly what we expect to happen in quantum phase transitions.

This paper is organized as follows: in the second section we analyze the eTMBH model through bifurcations in a classical analysis. These are used to indicate potential quantum phase transitions. We find the fixed points for the special case $\Delta = 0$, $U_1 = U_2$ and build a parameter space of phase transitions. A comparison is made between the classical predictions and the energy gap. In the third section we present the Bethe ansatz solution and investigate the distribution of the roots of the Bethe ansatz equations for the ground state. In the fourth section we summarize our results.

II. CLASSICAL ANALYSIS

We start our analysis with a semi-classical treatment. We study the phase space of this system, in particular determining the fixed points. It is found that for certain coupling parameters bifurcations of the fixed points occur, and we can determine a parameter space diagram which classifies the fixed points.

For this second-quantized model, if the particle number n is large enough, the system can be well described in the classical approximation [18], where creation/annihillation operators can be replaced by complex numbers $(n_j,\, \theta_j)$ such as

$$\hat{a}_j \to e^{i\theta_j}\sqrt{n_j},\;\; \hat{a}_j^\dagger \to \sqrt{n_j}e^{-i\theta_j}.$$

By introducing the canonically conjugate variables *population imbalance* z and *phase difference* θ, defined by

$$z = \frac{1}{n}\left(n_1 - n_2\right),\, \theta = \frac{n}{2}\left(\theta_1 - \theta_2\right),$$

the system can be described by the classical Hamiltonian

$$\mathcal{H} = \frac{nJ}{4}\left(\lambda\left(1+z^2\right) - \gamma\left(1-z^2\right)\cos\left(4\theta/n\right) - 2\sqrt{1-z^2}\cos\left(2\theta/n\right) - 2\beta z\right), \tag{2}$$

where

$$\lambda = \frac{n}{J}\left(U_1+U_2\right),\, \beta = \frac{n}{J}\left(\frac{\Delta}{n} - U_1 + U_2\right) \text{ and } \gamma = \frac{n\Omega}{J}$$

are the coupling parameters. Hamilton's equations of motion are given by

$$\dot{z} = -J\sin\left(2\theta/n\right)\left(2\gamma\cos\left(2\theta/n\right) - 2\gamma z^2\cos\left(2\theta/n\right) + \sqrt{1-z^2}\right) \tag{3}$$

$$\dot{\theta} = \frac{nJ}{2}\left(-\beta + \gamma z\cos\left(4\theta/n\right) + \frac{z\cos\left(2\theta/n\right)}{\sqrt{1-z^2}} + \lambda z\right) \tag{4}$$

In the limit $\gamma \to 0$ we recover the equations of motion of the TMBH [19]. The fixed points can be readily derived from the condition $\dot{z} = \dot{\theta} = 0$. Due to periodicity of the solutions, below we restrict to $2\theta/n \in [-\pi, +\pi]$. This leads to the following classification:

- $\theta = 0$ and z is a solution of

$$-\beta + z\left(\gamma+\lambda\right) = -\frac{z}{\sqrt{1-z^2}}, \tag{5}$$

  which has one solution for $\lambda+\gamma \geq -1$ while may have one, two or three solutions for $\lambda+\gamma < -1$. In Figure 1 we present a graphical solution of (5).

- $2\theta/n = \pm\pi$ and z is a solution of

$$-\beta + z\left(\gamma+\lambda\right) = \frac{z}{\sqrt{1-z^2}}. \tag{6}$$

  This equation has one solution for $\lambda+\gamma \leq 1$ and has either one, two or three real solutions for $\lambda+\gamma > 1$.

- $z = \beta/\left(\lambda-\gamma\right)$ and θ is a solution of

$$\cos\left(2\theta/n\right) = \frac{-1}{2\gamma\sqrt{1-\left(\frac{\beta}{\lambda-\gamma}\right)^2}}, \tag{7}$$

  which has two real solutions for $\gamma \notin [-1/2,\, 1/2]$ and $|\lambda-\gamma| \geq 2|\beta\gamma|\left(4\gamma^2-1\right)^{-1/2}$.

From the equations (5) and (6) we can determine that there are fixed point bifurcations for certain choices of the coupling parameters. These bifurcations allow us to divide the coupling parameter space in three regions. A standard analysis shows the boundary between the regions obey the relation

$$\lambda+\gamma = \pm\left(1+|\beta|^{\frac{2}{3}}\right)^{\frac{3}{2}} \tag{8}$$

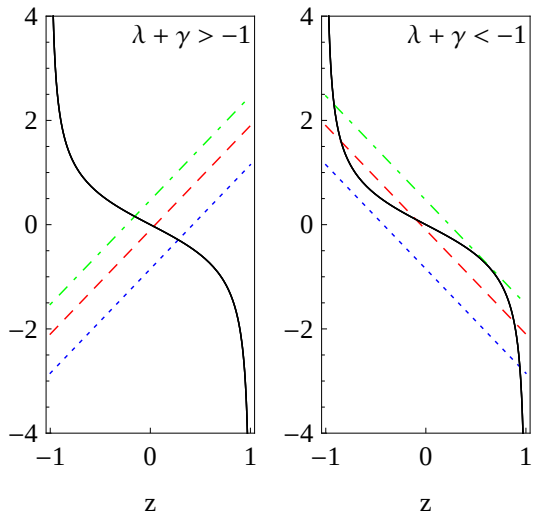

Figure 1. Graphical solution of equation (5). The crossing between the straight line (left hand side of eq. (5)) and the curve (right hand side of eq. (5)) for different values of $\lambda+\gamma$ and β represents the solution(s) for each case. There is just one solution on the left ($\lambda+\gamma \geq -1$) while there are either one, two or three solutions on the right ($\lambda+\gamma < -1$).

(see [20] for details). Eq. (8) leads to a partition of the parameter space into three regions, depicted in Figure 2a. In the absence of the external potential, i.e. $\beta = 0$, we have a fixed point bifurcation given by $\lambda = \pm 1 - \gamma$. See Figure 2b. Irrespective of the nature of the bifurcation, it has been observed in the classical analysis [21, 22] that fixed points can be used to identify quantum phase transitions. This model therefore becomes a promising candidate to study.

The conditions for existence of solutions to equation (7) allow us to build a parameter space diagram as depicted in Figure 2c. The boundary between regions satisfies the relation

$$\lambda - \gamma = \pm 2|\beta\gamma| \left(4\gamma^2 - 1\right)^{-1/2} \tag{9}$$

A. Fixed points and eigenstates for $\beta = 0$

In the following we will study the solutions of the fixed point equations (5), (6) and (7) with $\beta = 0$ by the consideration of two main reasons: (i) nonzero values of Δ do not significantly alter the behavior of the system, just shifting the energy levels [7] and (ii) much of the experimental realizations with these systems are made on the condition of zero external potential and equal interaction between atoms in each well [9]. In Figure 2b we see the parameter space diagram for equations (5) and (6) with $\beta = 0$, while Figure 2d shows the parameter space diagram for equation (7) for $\beta = 0$.

It has been demonstrated that the fixed points of phase-space level curves are the points of extreme energy

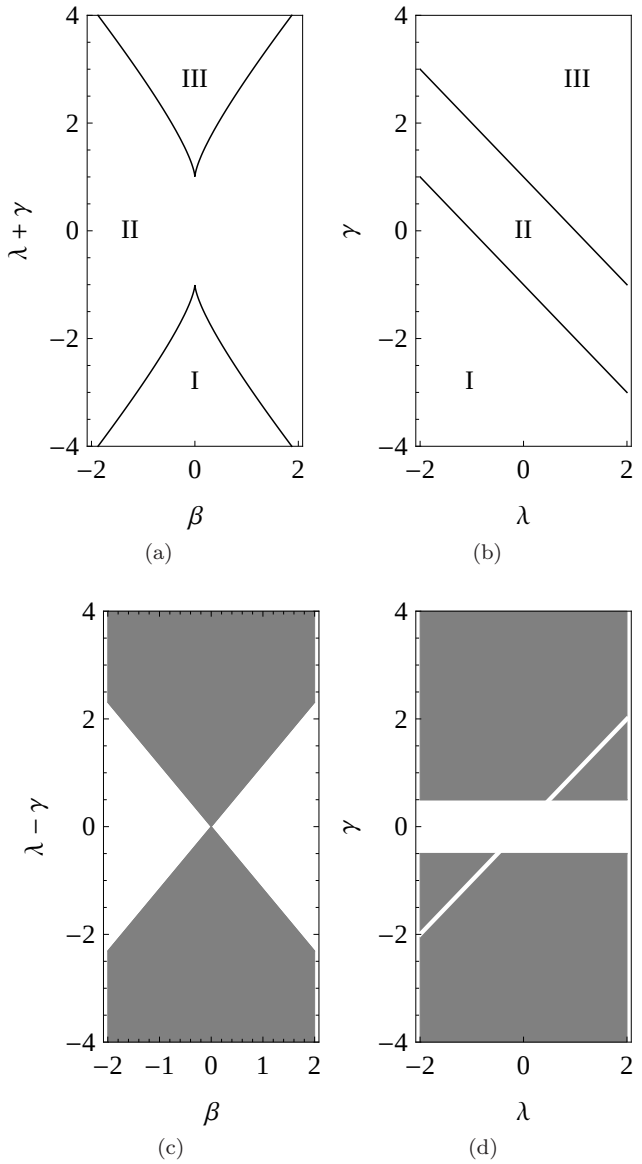

Figure 2. Coupling parameter space diagrams characterizing the solutions for the fixed points $\dot{z} = \dot{\theta} = 0$. (a) Parameter space for equations (5) and (6) with $\beta \neq 0$. The boundaries between the regions are given by equations (8). At the boundary between the regions I and II there are two solutions for $\theta = 0$ and one solution for $2\theta/n = \pm\pi$, while there is one solution for $\theta = 0$ and two solutions for $2\theta/n = \pm\pi$ at the boundary between regions II and III. (b) Parameter space for equations (5) and (6) with $\beta = 0$. The boundaries between the regions obey the equations $\gamma = \pm 1 - \lambda$. In both cases, there are three solutions for $\theta = 0$ and one solution $2\theta/n = \pm\pi$ in the region I; In the region II we have one solution for $\theta = 0$ and one solution for $2\theta/n = \pm\pi$; In the region III there is one solution for $\theta = 0$ and three solutions for $2\theta/n = \pm\pi$. (c) Example of parameter space for equation (7) with $\beta \neq 0$. This equation only has one solution for the values of parameters that lie within the shaded area, with boundaries given by (9), and $|\gamma| > 1/2$. (d) Parameter space for equation (7) with $\beta = 0$. This equation only has a solution for the values of parameters that lie within the light gray area, with $|\gamma| > \frac{1}{2}$ and $\gamma \neq \lambda$.

Region I	P_1	P_2	P_3	P_4	P_5
$\gamma < \lambda$	*lmax*	*sp*	*GS*	*HES*	—–
$-1/2 > \gamma > \lambda$	*lmax*	*GS*	*sp*	*HES*	—–
$-1/2 < \gamma < 1/2$	*sp*	*GS*	—–	*HES*	—–
$\gamma > 1/2$	*sp*	*GS*	*HES*	*sp*	—–

Table I. Configuration of fixed points and associated states in region I. In this table, GS means *Ground State*, lmax is a *local maxima*, sp is a *saddle point* while HES refers to the *Highest Excited State*.

corresponding to eigenstates of the system [23]. Since the fixed point bifurcations change the topology of the level curves, qualitative differences can be observed between each of the three regions. For further analysis, it is useful to assign to each fixed point $(\theta_{FP},\, z_{FP})$ a point P_j in the phase space as follows:

$$\begin{cases} P_1 \to (0,\, 0) \\ P_2 \to \left(0,\, \pm\sqrt{1 - 1/\left(\lambda+\gamma\right)^2}\right) \\ P_3 \to \left(\pm \text{arcsec}\left(-2\gamma\right),\, 0\right) \\ P_4 \to (\pm\pi,\, 0) \\ P_5 \to \left(\pm\pi,\, \pm\sqrt{1 - 1/\left(\lambda+\gamma\right)^2}\right) \end{cases}$$

Figure 3 shows the typical character of the level curves in region I. There are three fixed points for $\theta = 0$ and one fixed point for $2\theta/n = \pm\pi$. When $\gamma < \lambda$ the ground state is associated with the fixed points P_3. These two states are called *phase-locking states* with zero population imbalance and tunable relative phase unequal to 0 or π - see Figure 3a. This phase-locking state was also identified in [12]. Highest energetic states corresponds to the fixed points P_4. At $\gamma = \lambda$ the system changes to a special state: the ground state is over a "ring" instead a of point, as depicted in Figure 3b. This is a transition state, since any small changes in the values of λ and γ alter its nature. When $\gamma > \lambda$ there are an abrupt change in the ground state: the minima energy levels moves towards the fixed points P_2. We denote *self-trapping states* as those eigenstates whose corresponding fixed points have a nonzero population imbalance, $z \neq 0$, as depicted in Figure 3c. Therefore, now the ground state is a degenerate self-trapping state. This means that at $\gamma = \lambda$ the system undergoes a QPT from degenerate phase-locking states to degenerate self-trapping states. Further changes in the coupling parameters modify the fixed point configuration, but no longer alter the nature of the ground state. Table I provides a detailed classification for all the fixed points in region I as the parameters λ and γ change.

Figure 4a illustrates the configuration of the fixed points when the coupling parameters are tuned to cross

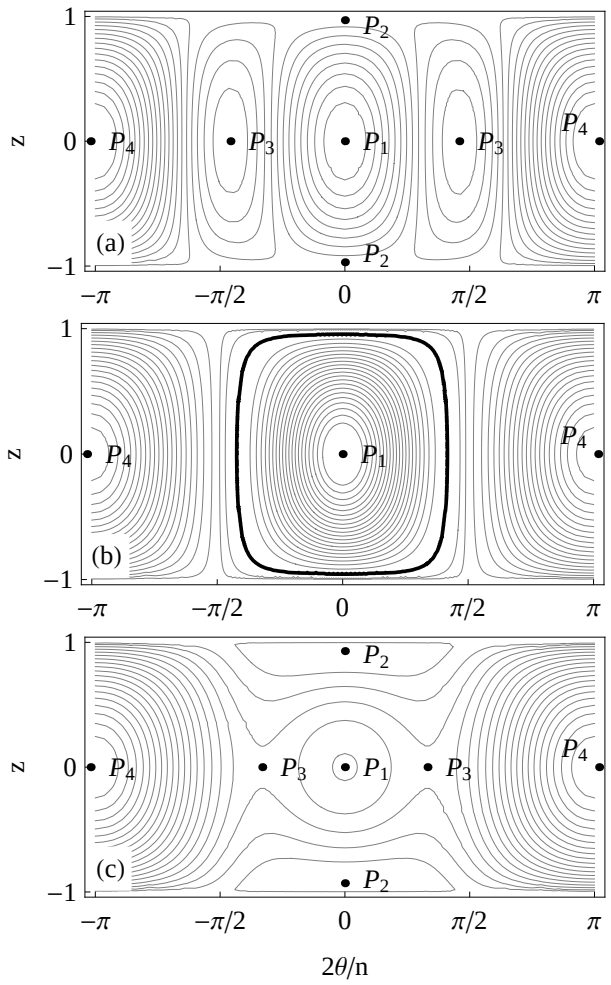

Figure 3. Level curves of the classical Hamiltonian in region I. The points $\{P_1, ..., P_4\}$ denote the fixed points of the Hamiltonian. (a) the parameter values are $n = 100$, $\lambda = -2$, $J = 1$ and $\gamma = -4$. There is a local maximum at P_1 and saddle points at P_2. Global minima are at P_3, while P_4 are global maxima. In (b) the parameter values are $n = 100$, $\lambda = -2$, $J = 1$ and $\gamma = -2$. A "ring" emerges as the global minimum. The local and global maxima still occur at P_1 and P_4, respectively. (c) Now the parameter values are $n = 100$, $\lambda = -2$, $J = 1$ and $\gamma = -1$. Global minima are at P_2. There are saddle points at P_3, a local maximum point at P_1 and global maxima at P_4.

over from region I into region II. There is one fixed point for $\theta = 0$ and one for $2\theta/n = \pm\pi$. If $\gamma > -1/2$ the fixed point P_1 becomes associated with the ground state, with zero population imbalance and zero relative phase, with the presence of tunnelling of atoms between the wells because of the weak interaction. We call this state a *Josephson state*. Therefore, when crossing the boundary $\gamma = -1 - \lambda$, the system undergoes a QPT to a non-degenerate Josephson state. Highest excited states are related to the global maxima at P_3. If $\gamma < -1/2$, there is another QPT: the global minima, related to degenerate phase-locking states, emerges at P_3 - see Figure 4b.

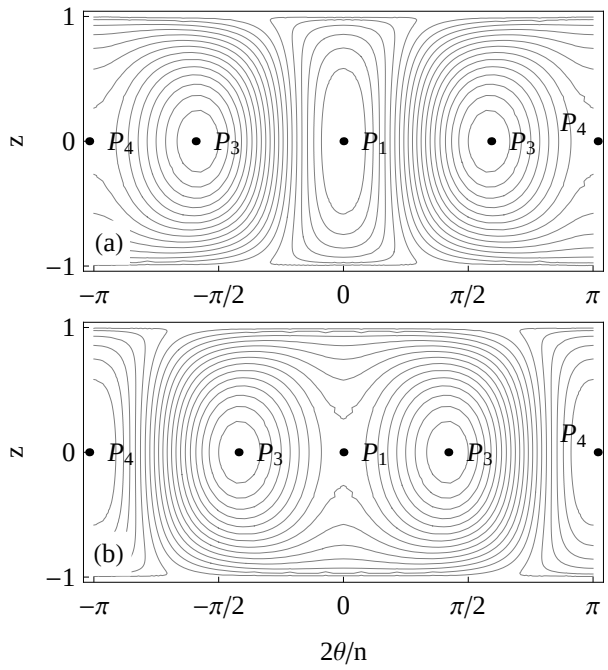

Figure 4. Typical level curves of the classical Hamiltonian in region II. The points $\{P_1, ..., P_4\}$ denote the fixed points of the Hamiltonian. (a) The parameter values are $n = 100$, $\lambda = -2$, $J = 1$ and $\gamma = 2$. There is a global minimum at P_1, global maxima is at P_3, while P_4 are saddle points. In (b) the parameter values are $n = 100$, $\lambda = 2$, $J = 1$ and $\gamma = -2$. Now the fixed point P_1 turns into a saddle point, while there are global minima at P_3 and global maxima emerge at P_4.

Region II	P_1	P_2	P_3	P_4	P_5
$-1/2 > \gamma$	*sp*	—	*GS*	*HES*	—
$-1/2 < \gamma < 1/2$	*GS*	—	—	*HES*	—
$\gamma > 1/2$	*GS*	—	*HES*	*sp*	—

Table II. Configuration of fixed points and associated states in region II. In this table, GS means *Ground State*, sp is a *saddle point* while HES refers to the *Highest Excited State.*

Highest energy states are associated with the fixed point P_4 for any $\lambda < 1/2$. Table II summarizes how the fixed point configurations change along with λ and γ.

On crossing the parameter space boundary to region III, the fixed point configuration change again: there is one fixed point for $\theta = 0$ and three fixed points for $2\theta/n = \pm\pi$. The ground state of the system may be associated with P_3 as a degenerate phase-locking state if $\gamma < -1/2$. New fixed points emerge at P_5 as highest energetic states. If $\gamma > -1/2$, the global minima changes to P_1 and becomes associated with a non-degenerate Josephson state. Therefore the line $\gamma = -1/2$ defines the boundary for a QPT - see Figure 5a and Figure 5b.

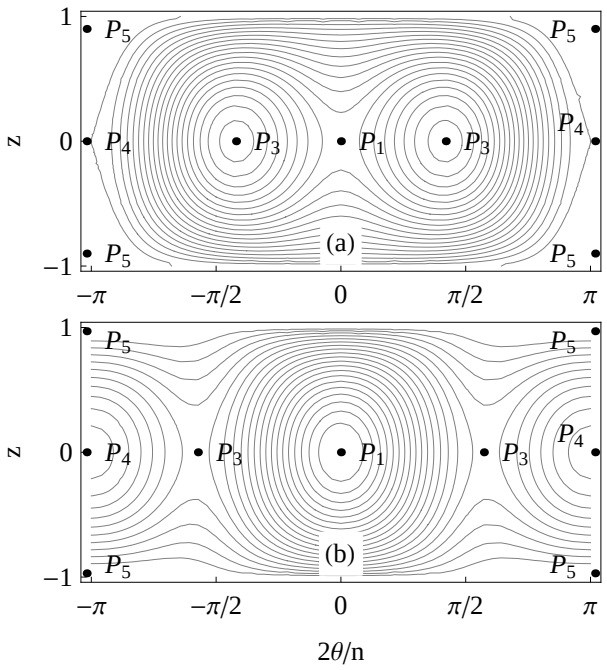

Figure 5. Typical level curves of the classical Hamiltonian in region III. The points $\{P_1, ..., P_5\}$ denote the fixed points of the Hamiltonian. In (a) the parameter values are $n = 100$, $\lambda = 4$, $J = 1$ and $\gamma = -2$. In this scenario P_1 is a saddle point and the global minima are at P_3. Highest energy levels appears at P_5. In (b) the parameter values are $n = 100$, $\lambda = 4$, $J = 1$ and $\gamma = 2$. Now the global minima move towards P_1 while P_3 become saddle points. The fixed points P_4 are local minima and the global maxima still at P_5.

Region III	P_1	P_2	P_3	P_4	P_5
$-1/2 > \gamma$	*sp*	—	*GS*	*sp*	*HES*
$-1/2 < \gamma < 1/2$	*GS*	—	—	*sp*	*HES*
$1/2 < \gamma < \lambda$	*GS*	—	*sp*	*lmin*	*HES*
$\gamma > \lambda$	*GS*	—	*HES*	*lmin*	*sp*

Table III. Configuration of fixed points and associated states in region III. In this table, GS means *Ground State*, lmin is a *local m*inima, sp is a *saddle point* while HES refers to the *Highest Excited State.*

The above discussion gives a general qualitative description of the behaviour of the classical system in terms of the three regions identified in the parameter space. Properties of eigenstates as highlighted in Tables I, II, and III enables us to depict the quantum phase transition diagram shown in Figure 6. The parameter space (λ, γ) is divided into three regions: self-trapping, Josephson, and phase-locking phases.

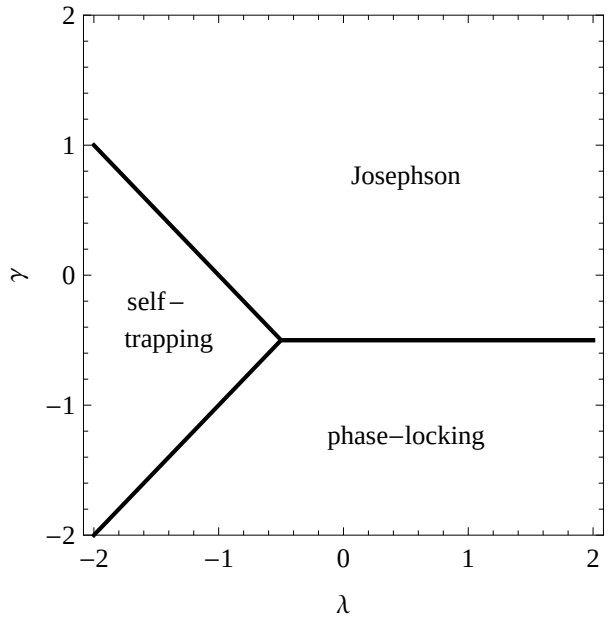

Figure 6. Parameter space for quantum phase transitions. The boundary between Josephson and phase-locking states is given by $\gamma = -1/2$. The system undergoes a QPT from phase-locking states to self-trapping states by crossing the boundary $\gamma = \lambda$, while the limit between the Josephson phase and the self-trapping phase is determined by the line $\gamma = -1-\lambda$. The threshold coupling occur at $(\gamma,\, \lambda) = (-1/2,\, -1/2)$.

In the next section we restrict ourselves to study the case $\lambda > 0$ and check the presence of a phase transition as predicted by the phase transition diagram studying the behaviour of the energy gap.

B. Energy gap

Consider the energy gap between the first excited state (FES) and the ground state (GS),

$$\Delta E = E_{FES} - E_{GS}. \tag{10}$$

The values of the parameters for which the gap goes to zero identifies the location of the QPT [24]. Using numerical diagonalization of the Hamiltonian (1), in Fig. 7a we plot the energy gap as a function of the coupling γ, for $\lambda > 0$ and different values of n. We observe that as n increases the energy gap decreases and the coupling approaches the point $\gamma = -1/2$. Fig. 7b shows similar results for fixed n and varying λ. We observe that the occurrence of the vanishing of the gap, determining the QPT, fits well with the predicted boundary separating Josephson and phase-locking regions given by $\gamma = -1/2$.

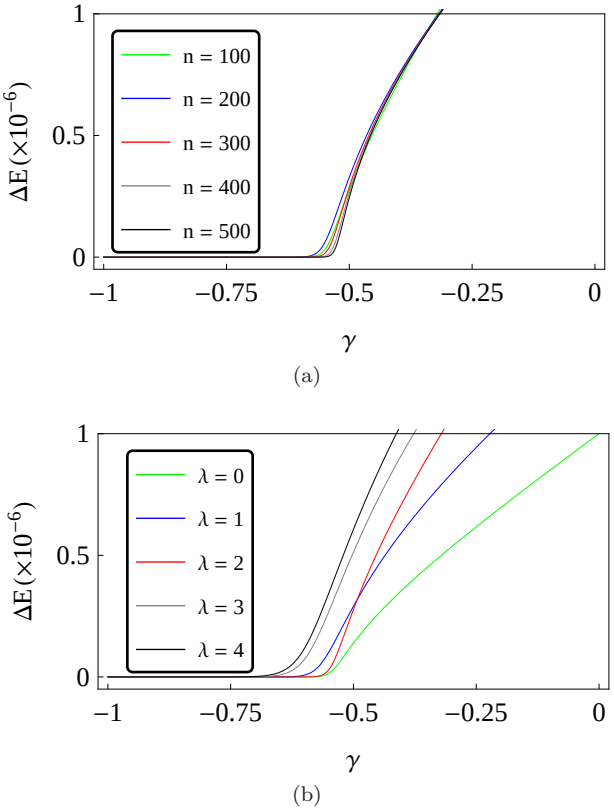

Figure 7. Energy gap between the first excited state and the ground state as a function of $\gamma = n\Omega/J$ for (a) different values of n and $\lambda = 2$ and (b) for different values of λ and $n = 100$. The values of the parameters are $J = 1$ and $\beta = 0$. These results indicate that the points at which the gap closes lie approximately on the line $\gamma = -1/2$.

III. BETHE ANSATZ SOLUTION

To obtain the exact solution of the eTMBH model, we follow the work of Enol'skii, Kuznetsov and Salerno [25]. Starting with the Jordan-Schwinger realisation of the $su(2)$ algebra:

$$\hat{S}^+ \to \hat{a}_1^\dagger \hat{a}_2,\ \hat{S}^- \to \hat{a}_2^\dagger \hat{a}_1,\ \hat{S}^z \to \frac{\hat{n}_1 - \hat{n}_2}{2}$$

we may write the Hamiltonian (1) as

$$H = \frac{k}{8}\hat{n}^2 + \frac{k}{2}\left(\hat{S}^z\right)^2 + \alpha\hat{S}^z - \frac{1}{2}J\left(\hat{S}^+ + \hat{S}^-\right) - \frac{1}{2}\Omega\left[\left(\hat{S}^+\right)^2 + \left(\hat{S}^-\right)^2\right] \tag{11}$$

with $\hat{n} = \hat{n}_1 + \hat{n}_2$, $k = 2\,(U_1 + U_2)$ and $\alpha = (U_1 - U_2)\,n - \Delta$. Note that

$$\lambda = \frac{kn}{2J},\ \beta = -\frac{\alpha}{J}. \tag{12}$$

If we consider the differential realization of su (2) operators,

$$\hat{S}^{+} \rightarrow nu - u^2 \frac{d}{du},\ \hat{S}^{-} \rightarrow \frac{d}{du},\ \hat{S}^{z} \rightarrow u\frac{d}{du} - \frac{n}{2}$$

the Hamiltonian (11) can be written as

$$H = A(u)\frac{d^2}{du^2} + B(u)\frac{d}{du} + C(u) \tag{13}$$

with

$$\begin{aligned} A(u) &= \frac{k}{2}u^2 - \frac{\Omega}{2}\left(u^4+1\right) \\ B(u) &= \frac{1}{2}\left\{J\left(u^2-1\right) + \left[k(1-n)+2\alpha\right]u \right. \\ &\quad \left. -2\Omega(1-n)u^3\right\} \\ C(u) &= \frac{k}{4}n^2 - \frac{\alpha}{2}n - \frac{J}{2}nu - \frac{\Omega}{2}n(n-1)u^2 \end{aligned}$$

Solving for the spectrum of the Hamiltonian is then equivalent to solving the eigenvalue equation

$$HQ(u) = EQ(u) \tag{14}$$

where H is represented by (13) and $Q(u)$ is a polynomial function of u of order n. Next, express $Q(u)$ in terms of its roots υ_j:

$$Q(u) = \prod_{j=1}^{n}(u - \upsilon_j)$$

Evaluating (14) at $u = \upsilon_l$ for each l leads to the set of Bethe ansatz equations (BAE)

$$\begin{aligned} &\frac{-J\left(\upsilon_l^2-1\right) + \left(k(1-n)+2\alpha\right)\upsilon_l - 2\Omega(1-n)\upsilon_l^3}{k\upsilon_l^2 - \Omega\left(\upsilon_l^4+1\right)} \\ &\quad = \sum_{j\neq l}^{n}\frac{2}{\upsilon_j - \upsilon_l} \end{aligned} \tag{15}$$

Writing the asymptotic expansion

$$Q(u) \sim u^n - u^{n-1}\sum_{j=1}^{N}\upsilon_j + u^{n-2}\sum_{j=1}^{n-1}\sum_{l=j+1}^{n}\upsilon_j\upsilon_l$$

and by considering the terms of order n in (14), the energy eigenvalues are found to be

$$E = \frac{kn^2}{4} + \frac{\alpha n}{2} - \frac{J}{2}\sum_{j=1}^{n}\upsilon_j - \Omega\sum_{j=1}^{n-1}\sum_{l=j+1}^{n}\upsilon_j\upsilon_l \tag{16}$$

Each set of roots $\{\upsilon_j,\ j = 1, ..., n\}$ of the BAE leads to an energy of the Hamiltonian through (16). Note that the change $J \rightarrow -J$ is equivalent to the change $\upsilon_j \rightarrow \upsilon_j^{-1}$. For $\alpha = 0$ this shows that each solution set $\{\upsilon_1, ..., \upsilon_n\}$ is invariant under $\upsilon_j \rightarrow \upsilon_j^{-1}$. In principle, an analytic solution of these equations is not possible. Below, we implement numerical techniques to obtain solutions.

We restrict ourselves to study the case $k > 0$, $\alpha = 0$ (due to the relations (12) this is equivalent to $\lambda > 0$, $\beta = 0$) to investigate the behaviour of the BAE solutions around the QPT line $\gamma = -1/2$. We start solving

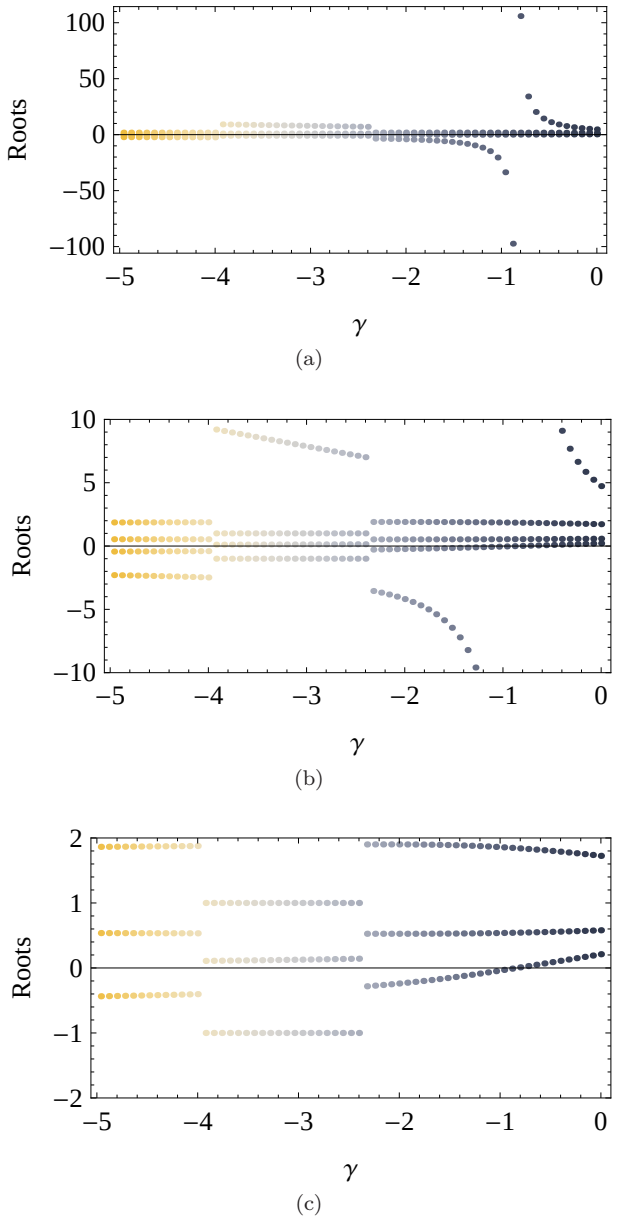

Figure 8. Solutions of BAE (15) for the ground state considering the particular case $n = 4$, $k = 1$ and $J = 1$ and different values of γ. The set of points with the same color is the solution of the BAE for a given value of γ. In (a), (b) and (c) we look at the same set of solutions in different scales. There are a abrupt change in the roots distribution occurring at $\gamma \simeq -2.38$ and $\gamma \simeq -4.01$.

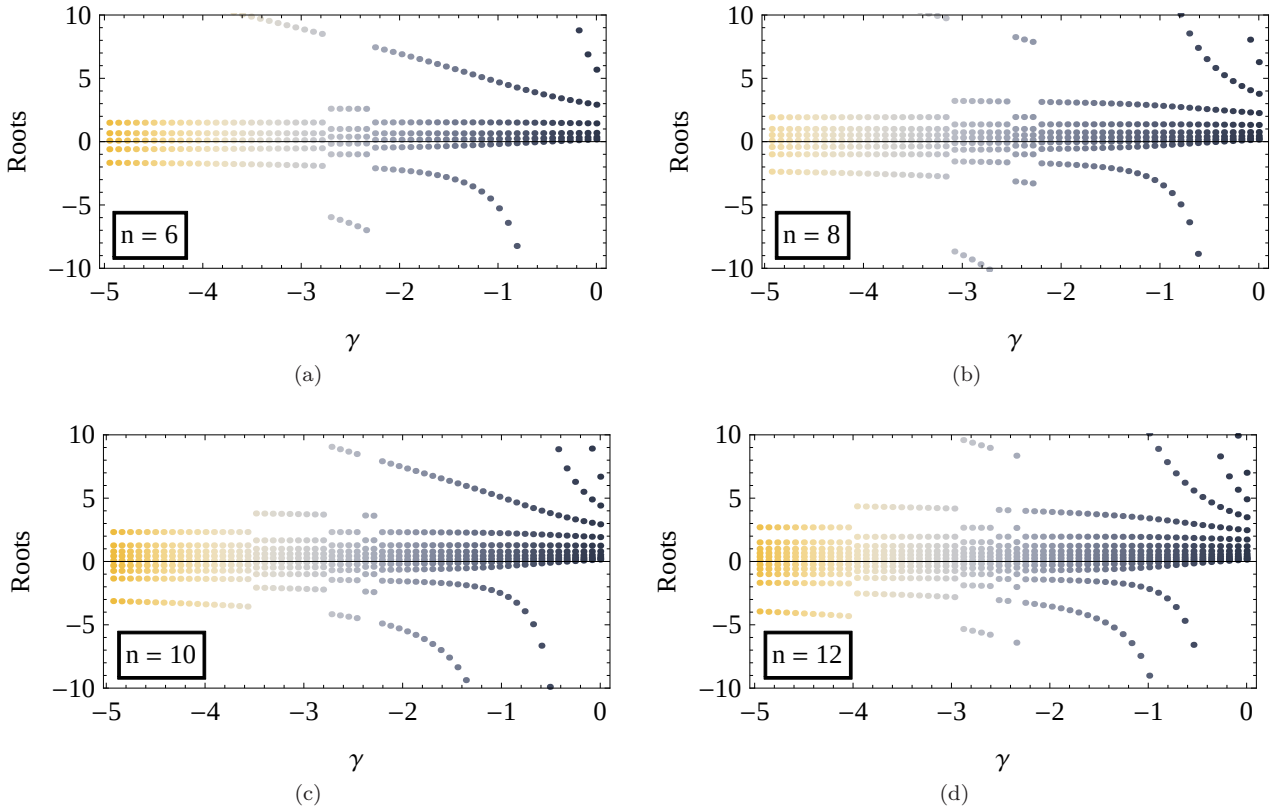

Figure 9. Solutions of BAE (15) for the ground state for $n = 6$, 8, 10 and 12, respectively. We set the parameters k and α to satisfy the condition $\lambda = 2$, $\beta = 0$ in each case. There are abrupt changes in the distribution of roots for all values of n. The changes occurs at (a) $\gamma \simeq -2.30$ and $\gamma \simeq -2.75$; (b) $\gamma \simeq -2.25$, $\gamma \simeq -2.54$ and $\gamma \simeq -3.12$, (c) $\gamma \simeq -2.25$, $\gamma \simeq -2.45$, $\gamma \simeq -2.75$ and $\gamma \simeq -3.54$; (d) $\gamma \simeq -2.25$, $\gamma \simeq -2.35$, $\gamma \simeq -2.54$, $\gamma \simeq -2.92$ and $\gamma \simeq -3.98$.

the Bethe ansatz equations with $\Omega = 0$ for the ground state. In this case, all the roots must be real and positive [26]. If we decrease the value of Ω, the numerical solution of the equations (15) shows that the ground state has always real roots, but eventually some roots have a smooth transition from positive to negative values. As some roots approach to zero, other ones diverge due the invariance $\upsilon_j \to \upsilon_j^{-1}$. It must be noted that this transition from positive to negative roots has no relation with the QPT of this model.

In Figures 8 and 9 we plot solutions of the BAE for certain values of the total number of particles n. These numerical solutions agree with the exact diagonalization of the Hamiltonian. Starting with Figure 8, we plot the solutions to the BAE (15) with $n = 4$. The roots generally evolve smoothly as the value of the parameter $\gamma = n\Omega/J$ varies, although for some particular values the trajectories exhibit jumps. This same characteristic behavior of the ground state roots is observed for other values of n - see Figure 9.

Examination of the energy levels of the system for small number of particles shows that there are crossings of levels between the ground state and the first excited state, detected due to the presence of non-zero regions in the energy gap. Note that the number of non-zero regions in the energy gap increases along with the number of particles, while it's amplitude becomes smaller (in fact, Figure 10 shows that the amplitute of the non-zero regions of the energy gap becomes $10\times$ smaller every time we add two particles to the system). We also note that, as the number of particles increases, the solutions of Bethe ansatz equations still predict the crossing of energy levels, despite the small value of ΔE.

IV. SUMMARY

In this work we introduced an eTMBH model with non-linear tunneling interaction term. We found that the model exhibits QPT between three different phases: a Josephson phase, a self-trapping phase and a phase-locking phase. This result was obtained through a classical analysis, allowing for the identification the parameter space of phase transitions as depicted in Fig. 6. For the case $\lambda > 0$, we compared the predictions coming from the classical analysis with the energy gap. It was found that the boundary between the Josephson and phase-locking regimes coincides with the closing of the gap.

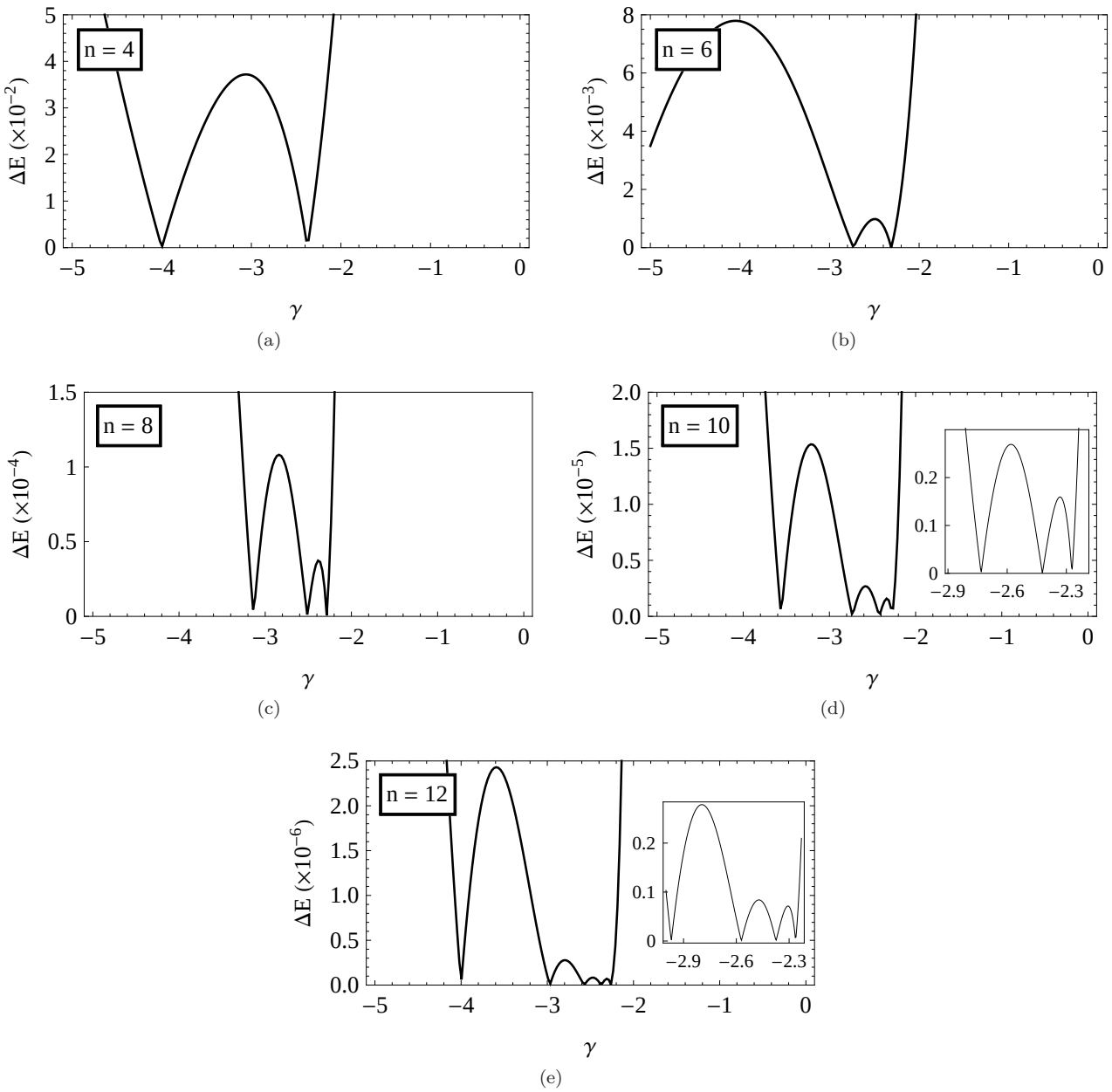

Figure 10. Energy gap between the ground state and the first excited state particular cases (a) $n = 4$, (b) $n = 6$, (c) $n = 8$, (d) $n = 10$ and (e) $n = 12$. We set the parameters $\lambda = 2$, $\beta = 0$ for all cases. The presence of non-zero regions in the energy gap indicates that there are level crossing between the ground state and the first excited state at some particular values of γ.

We then presented the exact solution for this model using the Bethe ansatz method. Guided by the location of quantum phase transition boundaries predicted by the classical analysis, we analysed solution of the BAEs and the energy gap. Crossing of levels between the ground state and the first excited state for a relatively small number of particles were detected. As we increase the number of particles, the crossings between these two levels becomes more frequent and with smaller amplitude of ΔE. The behaviour of the solutions for the BAE change at the points where the energy gap goes to zero.

The unusual features uncovered in this study call for a deeper analysis of the model. In future work it is planned to extend the methods adopted in [27, 28] for the TMBH model to meet this need.

V. ACKNOWLEDGEMENTS

Diefferson Rubeni and Angela Foerster are supported by CNPq (Conselho Nacional de Desenvolvimento Científico e Tecnológico), Brazil. Jon Links, Phillip Isaac and Angela Foerster are supported by the Australian Research Council through Discovery Project DP150101294.

[1] M. Albiez, R. Gati, J. Folling, S. Hunsmann, M. Cristiani and M. K. Oberthaler, Phys. Rev. Lett. **95** 010402 (2005).

[2] A. J. Leggett, Rev. Mod. Phys. **73**, 307 (2001).

[3] G. J. Milburn, J. Corney, E. M. Wright and D. F. Walls, Phys. Rev. A **55**, 4318 (1997).

[4] A. P. Hines, R. H. McKenzie and G. J. Milburn, Phys. Rev. A **67**, 013609 (2003).

[5] J. R. Anglin, P. Drummond, A. Smerzi, Phys. Rev. A **64**, 063605 (2001).

[6] H.-Q. Zhou, J. Links, R. H. McKenzie and X. -W. Guan, J. Phys. A: Math. Gen. **36**, L113 (2003) .

[7] A. P. Tonel, J. Links and A. Foerster, J. Phys. A **38**, 1235 (2005).

[8] F. Pan and J. P. Draayer, Phys. Lett. A **339**, 403 (2005).

[9] S. Fölling, S. Trotzky, P. Cheinet, M. Feld, R. Saers, A. Widera, T. Muller and I. Bloch, Nature **448**, 1029, (2007).

[10] S. Zöllner, H-D. Meyer and P. Schmelcher, Phys. Rev. Lett. **100**, 040401 (2008).

[11] D. Ananikian and T. Bergeman, Phys. Rev. A **73**, 013604 (2006).

[12] J-Q. Liang, J-L. Liu, W-D. Li and Z-T. Li, Phys. Rev. A **79**, 033617 (2009).

[13] J.-L. Liu and J.-Q. Liang, Mod. Phys. Lett. B **25**, 27, 2137–2148 (2011).

[14] J.-L. Liu and J.-Q. Liang, J. Phys. B: At. Mol. Opt. Phys. **44**, 025101 (2011).

[15] Q. Zhu, Q. Zhang and B. Wu, J. Phys. B: At. Mol. Opt. Phys. **48**, 045301 (2015).

[16] S. Dutta, A. Barman, A. Siddharth, A. Khan and S. Basu, Eur. Phys. J. B **88**, 139 (2015).

[17] L. Wen, Q. Zhu, T. Xu, X. Jing and C-S Liu, J. Phys. B: At. Mol. Opt. Phys. **49**, 015303 (2016).

[18] B. Wu, J. Liu, Phys. Rev. Lett. **96**, 020405 (2006).

[19] S. Raghavan, A. Smerzi, S. Fantoni and S. R. Shenoy, Phys. Rev. A **59**, 620-633 (1999).

[20] J. Links, A. Foerster, A. P. Tonel and G. Santos, Ann. Henri Poincare **7**, 1591-1600 (2006).

[21] A. P. Hines, R. H. McKenzie and G. J. Milburn, Phys. Rev. A **71**, 042303 (2005) .

[22] S. Schneider and G. J. Milburn, Phys. Rev. A **65**, 042107 (2002).

[23] L. Jie, W. Biao and N. Qian, Phys. Rev. Lett. **90**, 170404 (2003).

[24] S. Sachdev, Quantum Phase Transitions, Cambridge University, 2nd. edition, 2011.

[25] V. Z. Enol'skii, V. B. Kuznetsov, M. Salerno, Phys. D **68**, 138–152 (1993).

[26] J. Links and S-Y Zhao, J. Stat. Mech. P03013 (2009).

[27] D. Rubeni, E. Mattei, A. Foerster and I. Roditi, Nuc. Phys. B **853**, 698-715 (2011).

[28] J. Links and I. Marquette, J. Phys. A **48**, 4 (2015).

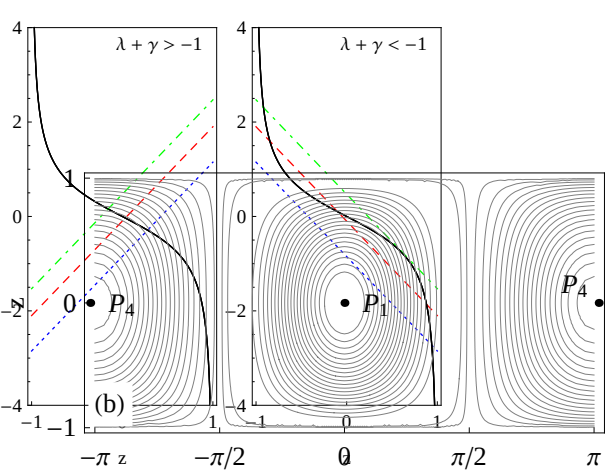
λ + γ > −1
λ + γ < −1
P4
P1
P4
(b)
−π
−π/2
0
π/2
π
z